Healing Effect of Controlled Anti-Electromigration on Conventional and High-T_c Superconducting Nanowires

Xavier D. A. Baumans, Joseph Lombardo, Jérémy Brisbois, Gorky Shaw, Vyacheslav S. Zharinov, Ge He, Heshan Yu, Jie Yuan, Beiyi Zhu, Kui Jin, Roman B. G. Kramer, Joris Van de Vondel, and Alejandro V. Silhanek*

The electromigration process has the potential capability to move atoms one by one when properly controlled. It is therefore an appealing tool to tune the cross section of monoatomic compounds with ultimate resolution or, in the case of polyatomic compounds, to change the stoichiometry with the same atomic precision. As demonstrated here, a combination of electromigration and anti-electromigration can be used to reversibly displace atoms with a high degree of control. This enables a fine adjustment of the superconducting properties of Al weak links, whereas in Nb the diffusion of atoms leads to a more irreversible process. In a superconductor with a complex unit cell ($La_{2-x}Ce_xCuO_4$), the electromigration process acts selectively on the oxygen atoms with no apparent modification of the structure. This allows to adjust the doping of this compound and switch from a superconducting to an insulating state in a nearly reversible fashion. In addition, the conditions needed to replace feedback controlled electromigration by a simpler technique of electropulsing are discussed. These findings have a direct practical application as a method to explore the dependence of the characteristic parameters on the exact oxygen content and pave the way for a reversible control of local properties of nanowires.

1. Introduction

The displacement of atoms caused by high electric current densities was already identified in the late 1960s as a major problem of narrow Al interconnects in integrated circuits and other electronic devices.[1] The negative perception of this phenomenon, known as electromigration (EM), has progressively changed during the last decades, as the scientific community first understood the physical mechanisms involved in the process and then learnt to master it.[2]

Examples illustrating the benefits of controlling the EM process include the creation of few nanometer gaps between

X. D. A. Baumans, J. Lombardo, J. Brisbois, Dr. G. Shaw, Prof. A. V. Silhanek
Experimental Physics of Nanostructured Materials
Q-MAT
CESAM
Université de Liège
B-4000 Sart Tilman, Belgium
E-mail: xavier.baumans@ulg.ac.be

V. S. Zharinov, Prof. J. Van de Vondel
INPAC – Institute for Nanoscale Physics and Chemistry
Department of Physics and Astronomy
KU Leuven, B-3001 Leuven, Belgium

DOI: 10.1002/smll.201700384

G. He, H. Yu, Prof. J. Yuan, Prof. B. Zhu, Prof. K. Jin
Beijing National Laboratory for Condensed Matter Physics
Institute of Physics
Chinese Academy of Sciences
Beijing 100190, China

Dr. R. B. G. Kramer
Université Grenoble Alpes
Institut NEEL
F-38000 Grenoble, France

Dr. R. B. G. Kramer
CNRS
Institut NEEL
F-38000 Grenoble, France

two Au pads[3] with the aim to electrically address single molecules,[4] the electrical sculping of nanowires to obtain atomic point contacts,[5] metal purification, and separation of atoms in binary alloys due to the mass selectivity of the process,[6] current-induced crystallization,[7] and cleaning of graphene layers.[8]

Arguably, one of the most appealing aspects of EM is the reversibility of the mechanism. Indeed, it has been shown that nanogaps, once created, can be closed by using voltage spikes[5a,9] while refilling of previously generated voids has been demonstrated in metals such as Al and Pd-Pt[10] by simply reversing the polarity of the dc current.

In this work, we introduce controlled EM as a powerful tool to explore superconducting nanoconstrictions. We show that this technique successfully works for Al, Nb, and $La_{2-x}Ce_xCuO_4$ (LCCO), three dissimilar superconductors. The reversed migration, here coined as anti-electromigration (anti-EM), allows us to heal the modifications previously produced by EM and to partially recover the original superconducting properties of the nanoconstriction. In addition, we establish the possibility to finely tune the resistance of an Al nanowire by using successive runs of EM/anti-EM. A similar effect is observed in nonconventional (cuprate-based compounds) superconducting microbridges, whereas it works only partially in Nb. In addition, we investigate an alternative controlled EM procedure consisting of electropulsing. This method is more accurate in terms of reaching the aimed resistance value, is faster than continuously monitoring EM, and much simpler to implement without the need of complex feedback control systems. The presented effects could be used as an appealing and interesting alternative for manipulating the superconducting properties of nanowires. Particularly relevant is the possibility to reversibly change the stoichiometry of high temperature superconductors without the need to fabricate different samples.

2. Results and Discussion

The investigation has been conducted on three different superconducting compounds, Al (T_c = 1.39 K), Nb (T_c = 8.7 K), and $La_{2-x}Ce_xCuO_4$ (LCCO, T_c = 26.1 K), covering a wide range of superconducting parameters (see the Experimental Section). All samples consist of a transport bridge with a central constricted section, as it is shown in **Figure 1** for Al [a,b], Nb [d,e], and LCCO [f–h]. The reduction of the width at the centre of the bridge is intended to increase the probability to migrate atoms in its vicinity. This is a natural consequence from the fact that electromigration is driven by temperature T and current density j as described by Black's formula for the mean lifetime of the nanowire[1d] τ given by $\tau = wtj^{-2}\exp\left(\frac{U}{k_B T}\right)$, where U is the activation energy needed to displace an atom, while w and t correspond to the width and thickness of the wire, respectively.

Figure 1c represents a simplified diagram of the main algorithm used to control EM. For all measurements presented in this work, the electromigration has been carried out in a cryogenic environment with bath temperature T_B just above the critical temperature of the concerned superconductor. More details about sample fabrication and EM software are given in the Experimental Section.

2.1. Electromigration of Al and Nb Nanoconstrictions

While electromigration of relatively large (several micrometers) Al bridges has been reported in Refs. [1b] and [10a,b] little is known about electromigration in nanoscale Al wires and constrictions. **Figure 2**a shows a typical evolution of the sample resistance, R, as a function of the applied current, I, during a controlled electromigration process of Al. The nearly parabolic increase of R with increasing I arises from the local increase of temperature due to Joule heating (see Supporting Information). For Al, this part of the $R(T)$ curve is nearly reversible and does not lead to significant mass transport. Electromigration takes place in the region where the current through the constriction diminishes while the resistance increases. This regime with negative dR/dI is irreversible and leads to permanent damage of the nanoconstriction as evidenced by the scanning electron microscopy (SEM) image shown in the inset of Figure 2e.

Notice that EM starts at $I \approx 5$ mA, corresponding to a maximum current density of 400 MA cm^{-2} at the narrowest point along the bridge. Based on Black's equation, we can conclude that the lower the T, the higher the J needed for achieving the point where dR/dI changes sign. This is confirmed by the linear relation between ln J and $1/T$ as shown in the inset of Figure 2g (see Supporting Information for details).

After the first EM shown in Figure 2a, the normal state resistance has increased by a factor of 3. Direct imaging of the induced damage is shown in the inset of Figure 2e. The $R(T)$ curve obtained in zero magnetic field condition and with an applied current I = 100 nA, much smaller than the one needed to initiate the EM, reveals a superconducting transition substantially broader than the one corresponding to the virgin sample shown with a dotted line in Figure 2e. This has been interpreted in terms of thermally activated phase slip phenomena[5c] (see Supporting Information).

The most interesting result is summarized in the second column of Figure 2. Panel (b) of Figure 2 shows that by inverting the direction of the electromigrating current, it is possible to anti-electromigrate, i.e., to reduce the resistance. A similar effect has been reported for Au and Pd–Pt nanowires.[10c] As shown in the inset of Figure 2f corresponding to the ex situ SEM image after anti-EM, the void has been refilled with material, naturally explaining the observed decrease in resistance. Figure 2f confirms that a sharp superconducting transition, very close to one of the initial virgin sample (dotted line in Figure 2e), is recovered after anti-EM. Extra sequences of EM (panels (c) and (g)) followed by anti-EM (panel (d) and (h)) unambiguously show the reversibility of this process in Al samples.

Further evidence of the controllability of the normal state resistance by alternating EM and anti-EM is shown in the inset of Figure 2h. Here, each resistance value achieved by EM differs from the targeted value by less than 0.25 Ω, demonstrating the fine tuning capability of the process.

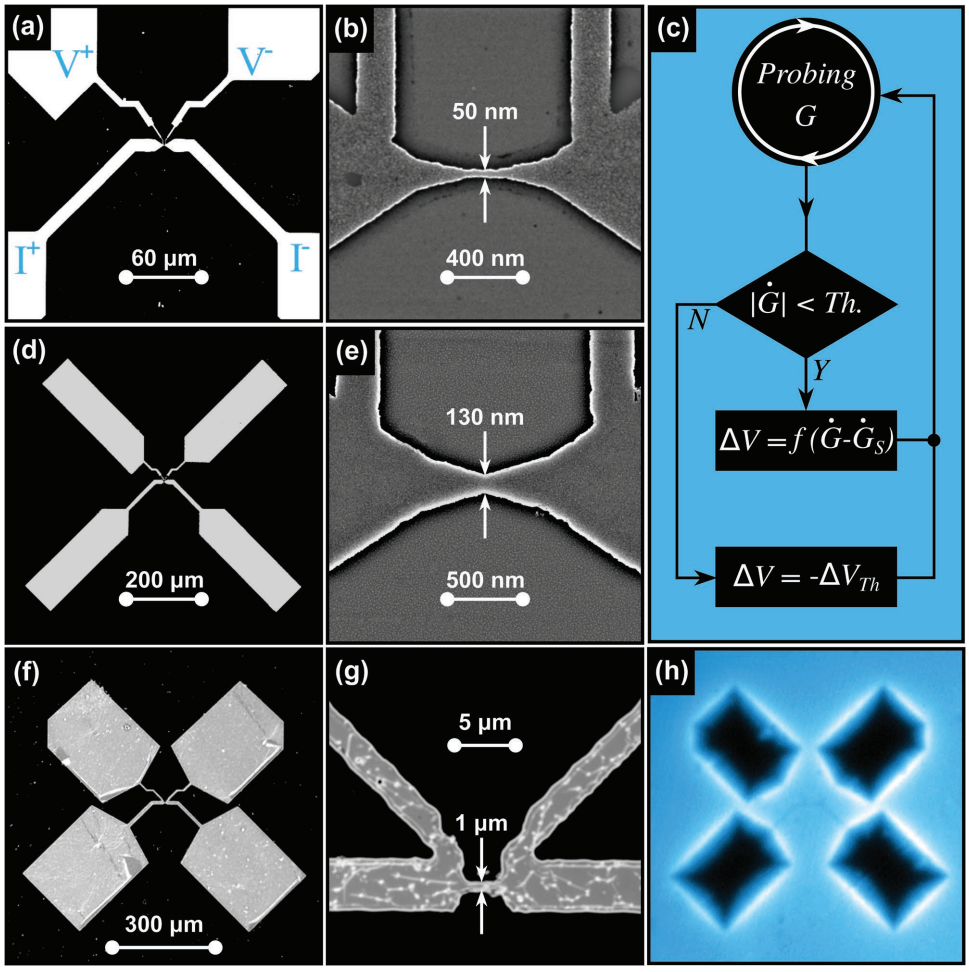

Figure 1. Sample layout and flowchart of the control feedback loop. a,b) Scanning electron microscopy images of the investigated Al samples obtained for two different magnifications. c) Schematic diagram of the algorithm used to achieve controlled electromigration. d,e) Scanning electron microscopy images of the investigated Nb samples obtained for two different magnifications. f,g) Optical microscopy images of the investigated LCCO samples at two different magnifications. h) Magneto-optical image of an LCCO sample obtained at $H = 1$ mT and $T = 3.6$ K, illustrating the smooth penetration of magnetic flux.

Considering that this process is realized in the very same sample, being reversible and with high level of control, it can be considered as an appealing approach to study the evolution of the physical properties of nanoconstrictions of different conducting materials. The question now arises as to whether Al is a particularly malleable material permitting this manipulation and if the observed behavior can be generalized to other compounds. In what follows we shall discuss the cases of Nb and LCCO and show that there are some particularities in the electromigration process which are unique to each material.

Let us first focus on the electromigration process in Nb. Figure 2i shows the evolution of the resistance of an Nb constriction during the EM process. The general aspect of the curve resembles the response of Al nanoconstrictions, but a more careful analysis permits us to identify two important differences. First, the initial increase of resistance is irreversible, leading to changes in the superconducting properties of the constriction. Second, the current at which dR/dI changes polarity (threshold of severe electromigration) is not sharply defined, but rather a smooth transition is observed. We estimate (see Supporting Information) that the temperature at the maximum applied current is $T \approx 760$ K. Figure 2j shows $R(T)$ curves obtained at low drives (1 μA) after different electromigration histories. The first electromigration (EM1), obtained after applying 8.4 mA, gives rise to an increase of the normal state resistance as well as a much broader transition than the virgin sample. This effect is very similar to the Al constrictions and can thus be attributed to the enhanced impact of thermal fluctuations. Interestingly, even though this EM has been carried out at a current smaller than the one corresponding to the transition to the $dR/dI < 0$ regime, a clear change in the material properties is still observed. SEM images acquired at this stage of the process show no hint of structural damage. Starting from this point, two consecutive attempts of anti-EM (EM2 and EM3) lead to a rather weak recuperation of the superconducting state, but producing no noticeable change in the normal state resistance. Changing the polarity of electromigration back into the initial condition and always dwelling within the regime where $dR/dI > 0$, we are able to further increase the normal state resistance and widen the superconducting transition as shown in EM4.

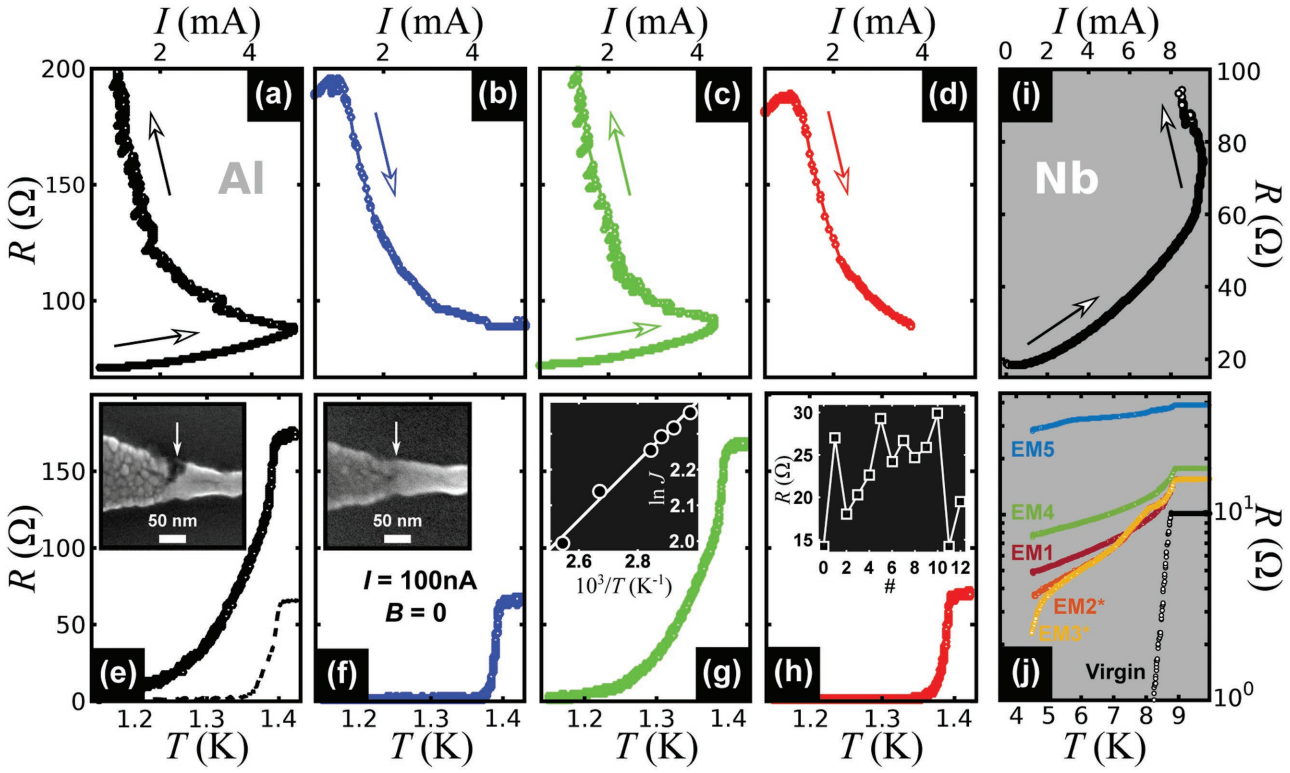

Figure 2. Anti-electromigration in a–h) Al and i,j) Nb nanowires. (a–d) Electromigration curves showing the evolution of resistance as a function of current for Al. Panels (e–h) show the $R(T)$ curves obtained after each EM (e,g) and anti-EM (f,h). Insets in (e) and (f) are scanning electron images evidencing the creation and healing of a void at the constriction of the nanowire. The dashed line in panel (e) shows the response of the virgin sample. The inset in panel (g) shows the linear relation between ln J and T^{-1}, for the (T, J) points corresponding to the maximum current density and local temperature. Inset in (h) represents the chronology of the resistance obtained during 12 successive runs of EM/anti-EM on the same nanowire at $T_B = 1.5$ K. Panel (i) shows the evolution of resistance as a function of current during an electromigration process for a Nb constriction. In (j) the resistance versus temperature obtained at low drives (1 μA) after a series of EM/anti-EM processes is shown. Numbers indicate the chronological order. Asterisks denote anti-electromigration runs.

The curve EM5 results from a severe electromigration in the $dR/dI < 0$ regime.

In general, we confirm that forward electromigration in Nb increases the resistance of the constriction whereas anti-EM produces very weak recovery of the superconducting properties. In other words, there is little influence of the current polarity on the final resistive state. This is in striking contrast to what is observed in Al. In Ref. [11] it was shown that O diffusion in Nb[12] becomes important above 400 K. Considering that the estimated sample temperature at the onset of electromigration lies largely above 400 K and that the chamber of the cryostat is not in ultrahigh vacuum conditions, it is plausible that O diffusion takes place during the EM. In addition, the strain along grain boundaries and defects is known to yield an enhanced O concentration and diffusion.[13] Based on this information and the presented experimental results, we envisage a scenario where EM in Nb occurs in two steps. At low currents, O atoms are subjected to migration thus leading to clear changes in the superconducting properties and the normal state resistance. In this regime, no noticeable changes of the structure are expected. At large bias currents ($dR/dI < 0$), Nb atoms can be displaced and a more conventional electromigration takes place.

Considering that the strong directional bond between Nb and O gives rise to large binding energies above 5 eV[14] it is interesting to verify our hypothesis in an alternative system where O atoms are more susceptible to displacements by an electron current. To that end, in the next section we focus our attention on a copper oxide superconducting compound.

2.2. Electromigration of LCCO Microconstrictions

Pioneer investigations of the electromigration of oxygen in a prototypical high critical temperature superconductor $YBa_2Cu_3O_{7-\delta}$ have been reported in Ref. [15]. Later on, Moeckly et al.[16] have explored this process in micrometer size bridges of the same material at room temperature. These authors reported an improvement of the normal and superconducting properties of the microbridge, raising J_c, and lowering the normal state resistivity by up to 30% for currents below a threshold bias of about 5 MA cm^{-2}. Above this threshold the transport properties were shown to rapidly degrade. The detrimental effects were attributed to the electromigration of basal-plane oxygen and the resultant formation of inhomogeneous oxygen deficient and disordered distributions giving rise to filamentary superconducting regions of nanometer scale within a nonsuperconducting background. Interestingly, the authors also reported that moderately damaged structures may be effectively restored

by subsequent application of a large DC current with the opposite polarity. In other words, similarly to the case described for Nb, the effect of EM is not to produce a morphological change but to create oxygen deficient regions.

We have extended these early investigations to a sister compound, $La_{2-x}Ce_xCuO_4$. In our case, the EM is carried out at low temperatures, allowing us to access a regime of rather cold electromigration. As shown in **Figure 3**a, the electromigration process resembles that of Nb, with an initial parabolic shape of the $R(I)$ characteristic followed by a smooth transition to the region where $dR/dI < 0$. Along the region where $dR/dI > 0$, the response is reversible as in Al. In the region of negative slope the response is irreversible although it generates no visible damage to the structure. This is shown by comparing the SEM images corresponding to the virgin sample in **Figure 4**a to that of the same sample after electromigration in the negative slope regime (see Figure 4b). If, however, very high current densities are applied, a clear imprint of the damage caused in the structure is observed, as indicated by the arrow in Figure 4c after applying 80 MA cm^{-2}. We argue

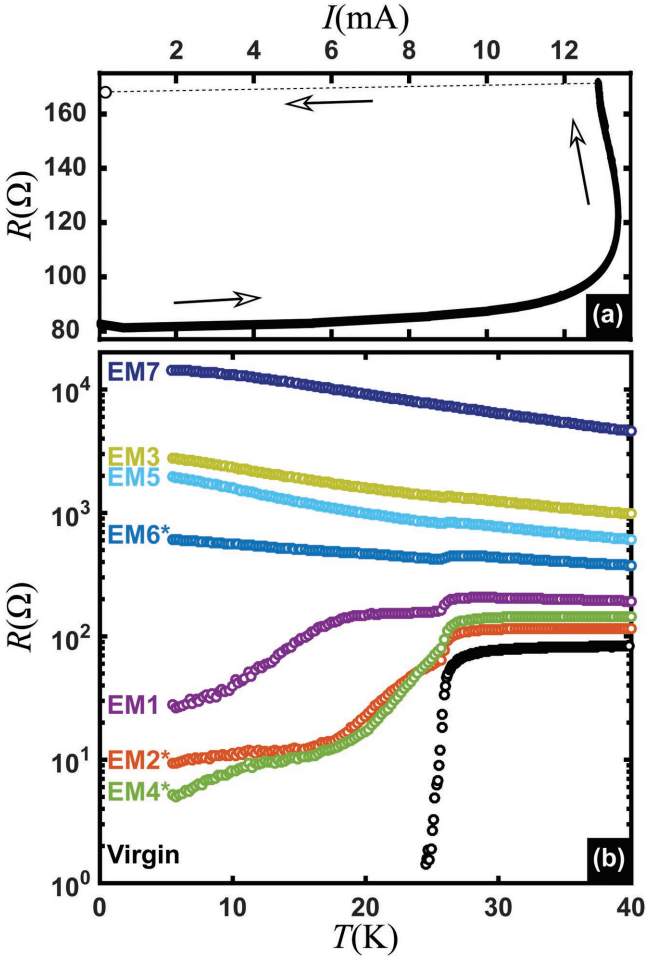

Figure 3. Electromigration-healing sequences in LCCO microwires. a) Typical $R(I)$ response during an electromigration process in LCCO at a bath temperature of 30 K. Upper left point denotes the value of the resistance measured after the electromigration run. b) Resistance versus temperature characteristics of a LCCO microbridge after successive electromigrations. Numbers indicate the chronological order. Asterisks denote anti-electromigration runs.

that at relatively low current densities, only oxygen atoms are displaced by the electron wind, whereas at sufficiently high current densities heavier atoms are able to migrate within the unit cell. In addition, in our polycrystalline LCCO sample, highly strained grain-boundary regions may contain excess O vacancies as reported for YBCO,[17] and can further influence the change of local oxygen doping via electromigration.

Evidence of the irreversible response obtained after electromigration with weak currents is shown in Figure 3b where the $R(T)$ characteristics obtained with a bias current $I = 1$ μA are shown after successive electromigrations. The virgin sample, i.e., before electromigration, exhibits a superconducting transition at about 26 K. After the first electromigration process (EM1) the normal state resistance has been increased by 110 Ω and the superconducting transition defined at 50% criterion, has diminished by a factor of 1.7. This change can be partially healed by reversing the current direction (EM2*). If the resistance of the constriction is brought above 350 Ω the superconducting transition is no longer present in the range of temperatures here investigated. Instead, an increase of resistance with decreasing T, characteristic of an insulating state, is observed. Interestingly, the superconducting state can still be recovered by anti-EM (see curve EM4*).

To our knowledge, this is the first evidence of a current-driven superconductor-insulator transition (SIT) in LCCO films. In order to dig into the possible scenarios describing the mechanism behind these phenomena, let us first remind some important facts concerning these materials. Electron-doped LCCO is in the so-called T' structural phase, while the hole-doped counterpart $(La,Sr)_2CuO_4$ (LSCO) has a T-type structure. In the T-phase, one Cu atom and six oxygen atoms form an octahedron, whereas in the T'-phase the two apical oxygens are removed or moved to the rare-earth blocks (see Figure 1 in Ref. [18]). YBCO has a T^* structure, where only one apical oxygen is detached from the octahedron. Interestingly, a T'-to-T structural transition with tuning pressure was observed in $(Pr,Ce)_2CuO_4$, accompanied with a superconductor-insulator transition[19] which might suggest that large current densities can play the same role as pressure on oxygen migration. Another plausible interpretation of the reversible SIT is that oxygen is pushed away from the original position under high current density, resulting in a gradual distortion of the lattice along the bridge. This is consistent with the increase of the residual resistivity with increasing oxygen content as reported in Ref. [18]. A similar electrically driven redox reaction and the associated structural change has been observed in Ce oxides.[20] We should also mention that the reversible change of the bridge resistance could be associated with the resistive switching observed in transition metal oxides, for which the generation of oxygen vacancies has been identified as one of the possible mechanisms. Clearly, further investigations are needed to discern which among the above listed phenomena, is the dominant one.

It is worth noting that the transition point where dR/dI changes sign takes place at a critical current density of 13 MA cm^{-2} when done at a bath temperature of 50 K. We estimate a resistivity $\rho \approx 150$ μΩ cm for the LCCO films at 50 K and an RRR = 5.3 corresponding to $\alpha = 17.3 \times 10^{-3}$ K^{-1}.

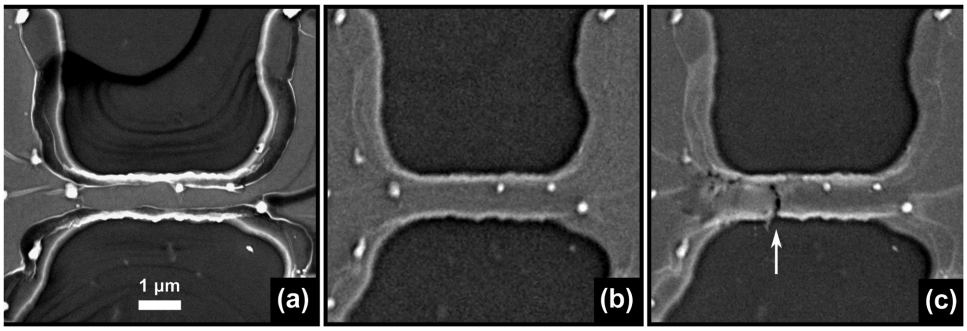

Figure 4. Structural characterization of electromigration in LCCO microbridge. a) Scanning electron image of virgin high-T_c microbridge. b) Image of the same bridge as in (a), taken after electromigration (EM2). c) Very last state of the bridge taken after having applied high voltage to increase resistance until measuring current values characteristic of tunneling.

From these parameters we can estimate that the maximum temperature during the electromigration is $T \approx 70$ K (see Supporting Information).

Finally, it is interesting to consider the possibility that the critical current density of a superconductor can exceed the density of current needed for EM. This may be achieved in high critical temperature superconductors like YBCO where $J_c \approx 3$ MA cm^{-2} at 77 K and $J_c \approx 30$ MA cm^{-2} at 10 K. Since these values of current densities lie above the current needed to migrate oxygen atoms, in case the dissipative regime of the superconductor is reached, EM takes place and the properties of the material change irreversibly. Notice as well that if the stoichiometry of the compound is detuned by current, also the carrier density should be affected. We are not aware of studies addressing these issues.

2.3. Electropulsing

As we have pointed out above, severe electromigration starts at the point where dR/dI diverges, i.e., where a transition from dR/dI > 0 to dR/dI < 0 takes place. It is important to emphasize that this transition results from the reaction to the feedback signal and therefore its degree of abruptness reflects the speed with which this feedback control needs to operate. In other words, more pronounced is the curvature of the $R(I)$ at the transition, faster the feedback loop needs to react. The electromigrations performed in Nb (Figure 2i) and LCCO (Figure 3a) exhibit a rather smooth transition suggesting that the EM process corresponds to a progressive damage instead of an explosive phenomenon. This finding encouraged us to propose the simpler method of electropulsing[7] as an alternative to achieve controlled electromigration, without the need of costly and complex feedback systems. This approach consists in applying voltage pulses of magnitude similar to that needed to reach the critical current density of the virgin structure during a short period of time. The results obtained through this technique are summarized in **Figure 5**.

The main panel of Figure 5 shows the evolution of the final resistance of the constriction after a series of voltage pulses of amplitude 15 V and duration 1 s. The initial resistance of the sample (300 Ω) was first increased up to 1100 Ω and subsequently reduced to its initial value by applying pulses of negative polarity. A similar procedure applied to Nb (see inset of Figure 5) shows an increase of the initial resistance by a factor of 7. Pulses of negative polarity in Nb lead to very weak healing effects (not shown), in agreement with the electromigration results obtained by controlled feedback in this material.

We should mention that due to the rather abrupt transition observed in the electromigration curve of Al, electropulsing in this material requires a very short dwell time and very well-tuned voltage pulses. Attempts of achieving electropulsing in Al with few seconds scale pulses lead to immediate irreversible damage and the creation of nm scale gaps, similar to those reported in Refs. [5a] and [9] for Au nanowires. Note that increasing the duration of the pulse allows to increase the local temperature at the electromigrated spot, which leads to an exponential change in the probability to induce damage, as suggested by Equation (S1) of the Supporting Information. On the other hand, increasing the amplitude of the voltage pulse increases the current density at the constriction which appears quadratically in Equation (S1) of the Supporting Information. We have succeeded in obtaining partial EM of Al constrictions by using pulses shorter than ms scale and by varying the amplitude of the pulse.

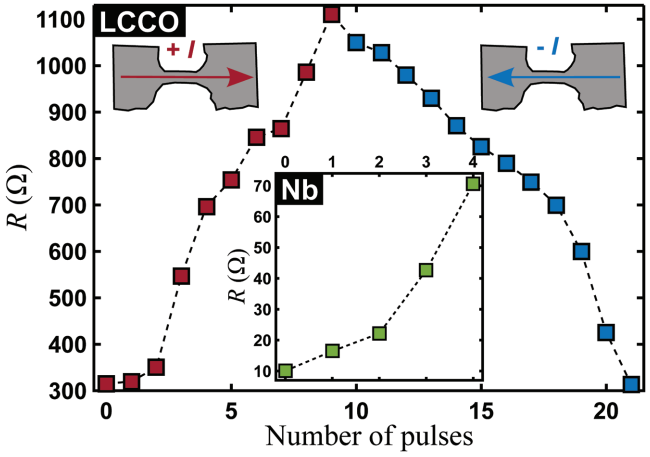

Figure 5. Electropulsing. Main panel: values of resistance obtained after applying voltage pulses to an LCCO microbridge. Amplitude and duration of a single pulse were respectively 15 V and 1 s. Red points are taken after pulses of same polarity, blue points are taken after pulses of reversed polarity. Inset: same as in main panel but for Nb.

3. Conclusion

In conclusion, we investigated the benefits of controlled electromigration and its healing counterpart as a knob to adjust the normal state resistance of preindented superconducting nanoconstrictions down to fractions of Ohms. The forward electromigration works for the three investigated superconducting materials, whereas healing effects exhibit a material dependent performance. While EM in Al always leads to structural changes at the nanoconstriction, in Nb and $La_{2-x}Ce_xCuO_4$ there is a regime at low current densities where an irreversible response is observed but without associated structural damage. We attribute this effect to the selective electromigration of oxygen atoms. We also discuss the possibility to achieve rather efficient controlled electromigration by electropulsing, which can be straightforwardly implemented without investing efforts in costly analogue feedback systems or complex software controlled feedback loops. We highlight the appealing aspect of electromigration for investigating superconducting nanoconstrictions, with the possibility to beat the state-of-the-art lithography methods complemented by the reversibility of the process. We illustrate this fact by unveiling for the first time a current induced superconductor-to-insulator transition in $La_{2-x}Ce_xCuO_4$.

4. Experimental Section

Aluminum samples were patterned by electron beam lithography on an Si/SiO_2 substrate (750 ± 50 µm Si, 300 ± 25 nm SiO_2) covered by a double layered PMMA resist mask, using a nanofabrication system from Raith GmbH. Subsequently, an Al thin film (≈25 nm) was deposited using molecular beam epitaxy with a deposition rate of 1 Å s^{-1} and a pressure in the chamber under 10^{-8} mbar. The deposition was followed by a lift-off process. Scanning electron images showing the sample layout with different magnifications are shown in Figure 1a,b. Figure 1c sketches the combined digital feedback loops used to carry out controlled electromigration. It consists of two algorithms working in parallel while ramping up the voltage: one intended to stabilize the EM rate and another to prevent thermal runaways in case of fluctuations in the junction. In that context, "Th" represents the threshold rate defining thermal runaway, $f(\dot{G}-\dot{G}_S)$ the feedback function minimizing $|(\dot{G}-\dot{G}_S|$, $\dot{G}_S$ the desired EM rate (set-point), and ΔV_{Th} the bias change needed to damp the thermal runaway.

The Nb samples with a thickness of 50 nm were deposited by electron beam evaporation under a pressure of 10^{-8} mbar at a rate of 1.5 Å s^{-1}. On top of it, 5 nm of Si was deposited for protecting the samples (pressure of 3×10^{-9} mbar and rate of 0.5 Å s^{-1}). The lithographic electron exposure was carried out in a Nanobeam nB5 platform with an electron beam energy of 80 keV. Afterward, an aluminum mask was fabricated by e-beam evaporation, followed by a lift-off. To remove the Nb not covered by the aluminum, reactive ion etching was performed using SF_6 during 10 s. Finally, the aluminum was removed using the base developer MF-26A. Scanning electron images showing the sample layout with different magnifications are shown in Figure 1d,e. The initial constriction width was about 130 nm, as indicated on Figure 1e.

The 100 nm thick high-T_c (LCCO) films were grown on (001)-oriented $SrTiO_3$ substrates by pulsed laser deposition, at temperatures ranging from 720 to 760 °C in an atmosphere of 0.13 mbar of pure oxygen. After the deposition, the films were annealed at the same temperature in vacuum for a few minutes to remove the excess of apical oxygen atoms, which are harmful to the superconductivity of electron-doped superconductors. The films were then slowly cooled down to room temperature in vacuum and finally patterned into microbridges by photolithography and Ar ion beam etching. Optical microscope images of the complete layout and the microconstriction are shown in Figure 1f,g, respectively. The white lines and dots observed in Figure 1g correspond to leftovers of the polymer resist mask and have no influence on the superconducting properties of the system. Figure 1h shows a magneto-optical image of an LCCO microbridge, evidencing a smooth penetration of magnetic flux into the sample. Dark areas correspond to low fields, while blue-white regions represent high fields. The homogeneity of the penetration is a strong indication of the high quality of the film, confirming excellent superconducting behavior and absence of macroscopic defects. More information about the magneto-optical setup can be found in Ref. [21].

Supporting Information

Supporting Information is available from the Wiley Online Library or from the author.

Acknowledgements

This work was supported by the Fonds de la Recherche Scientifique – FNRS, the Methusalem Funding of the Flemish Government and the Fund for Scientific Research-Flanders (FWO-Vlaanderen). J.V.d.V. acknowledges support from the KULeuven Internal Funds under Project No. CREA/14/011. J.B. (Research Fellowship) and J.L. (FRIA grant) acknowledge support from F.R.S.-FNRS. The work of G.S. was supported by the University of Liège and the EU in the context of the FP7-PEOPLE-COFUND-BeIPD project. The work of A.V.S. has been supported in part by PDR T.0106.16 of F.R.S.-FNRS. The authors thank the ULg Microscopy facility CAREM for part of the SEM investigations. K.J. acknowledges support from the National Natural Science Foundation of China (Grant No. 11474338). The LANEF framework (ANR-10-LABX-51-01) and the Nanoscience Foundation are acknowledged for their support with mutualized infrastructure.

Conflict of Interest

The authors declare no conflict of interest.

[1] a) P. B. Ghate, *Appl. Phys. Lett.* **1967**, *11*, 14; b) I. A. Blech, E. S. Meieran, *Appl. Phys. Lett.* **1967**, *11*, 263; c) R. Rosenberg, L. Berenbaum, *Appl. Phys. Lett.* **1968**, *12*, 201; d) J. R. Black, *Proc. IEEE* **1969**, *57*, 1587.

[2] a) F. d'Heurle, I. Ames, *Appl. Phys. Lett.* **1970**, *16*, 80; b) I. A. Blech, *J. Appl. Phys.* **1976**, *47*, 1203; c) P. S. Ho, T. Kwok, *Rep. Prog. Phys.* **1989**, *52*, 301; d) M. Saka, *Metallic Micro and Nano Materials*, Springer, NY, USA **2011**.
[3] a) M. F. Lambert, M. F. Goffman, J. P. Bourgoin, P. Hesto, *Nanotechnology* **2003**, *14*, 772; b) G. Esen, M. S. Fuhrer, *Appl. Phys. Lett.* **2005**, *87*, 263101; c) D. R. Strachan, D. E. Smith, D. E. Johnston, T.-H. Park, M. J. Therien, D. A. Bonnell, A. T. Johnson, *Appl. Phys. Lett.* **2005**, *86*, 043109; d) D. R. Strachan, D. E. Smith, M. D. Fischbein, D. E. Johnston, B. S. Guiton, M. Drndic, D. A. Bonnell, A. T. Johnson, *Nano Lett.* **2006**, *6*, 441; e) M. L. Trouwborst, S. J. v. d. Molen, B. J. v. Wees, *J. Appl. Phys.* **2006**, *99*, 114316.
[4] a) H. Park, J. Park, A. K. L. Lim, E. H. Anderson, A. P. Alivisatos, P. L. McEuen, *Nature* **2000**, *407*, 57; b) J. Park, A. N. Pasupathy, J. I. Goldsmith, C. Chang, Y. Yaish, J. R. Petta, M. Rinkoski, J. P. Sethna, H. D. Abrua, P. L. McEuen, D. C. Ralph, *Nature* **2002**, *417*, 722; c) L. H. Yu, D. Natelson, *Nano Lett.* **2004**, *4*, 79.
[5] a) N. Ittah, I. Yutsis, Y. Selzer, *Nano Lett.* **2008**, *8*, 922; b) J. M. Campbell, R. G. Knobel, *Appl. Phys. Lett.* **2013**, *102*, 023105; c) X. D. A. Baumans, D. Cerbu, O.-A. Adami, V. S. Zharinov, N. Verellen, G. Papari, J. E. Scheerder, G. Zhang, V. V. Moshchalkov, A. V. Silhanek, J. Van de Vondel, *Nat. Commun.* **2016**, *7*, 10560.
[6] W. Seith, S. Wever, *Z. Elektrochem.* **1953**, *57*, 891.
[7] a) T. Aref, A. Bezryadin, *Nanotechnology* **2011**, *22*, 395302; b) H. Mizubayashi, T. Takahashi, K. Nakamoto, H. Tanimoto, *Mater. Trans.* **2007**, *48*, 1665.
[8] J. Moser, A. Barreiro, A. Bachtold, *Appl. Phys. Lett.* **2007**, *91*, 163513.
[9] C. Xiang, J. Y. Kim, R. M. Penner, *Nano Lett.* **2009**, *9*, 2133.
[10] a) Z. Li, C. L. Bauer, S. Mahajan, A. G. Milnes, *J. Appl. Phys.* **1992**, *72*, 1821; b) C.-F. Hong, M. Togo, K. Hoh, *Jpn. J. Appl. Phys.* **1993**, *32*, L624; c) T. Kozlova, M. Rudneva, H. W. Zandbergen, *Nanotechnology* **2013**, *24*, 505708.
[11] J. Halbritter, *Appl. Phys. A* **1987**, *43*, 1.
[12] W. DeSorbo, *Phys. Rev.* **1963**, *132*, 107.
[13] a) H. Shiraishi, K. Furuya, R. Watanabe, *J. Less-Common Met.* **1979**, *63*, 147; b) M. Murakami, T. Yogi, *J. Appl. Phys.* **1985**, *57*, 211.
[14] a) A. K. Vijh, *J. Electrochem. Soc.* **1969**, *116*, 972; b) A. K. Vijh, *Oxid. Met.* **1972**, *4*, 63.
[15] a) K. G. Rajan, P. Parameswaran, J. Janaki, T. S. Radhakrishnan, *J. Phys. D: Appl. Phys.* **1990**, *23*, 694; b) S. Vitta, M. A. Stan, J. D. Warner, S. A. Alterovitz, *Appl. Phys. Lett.* **1991**, *58*, 759.
[16] a) B. H. Moeckly, R. A. Buhrman, *IEEE Trans. Appl. Supercond.* **1993**, *3*, 2038; b) B. H. Moeckly, D. K. Lathrop, R. A. Buhrman, *Phys. Rev. B* **1993**, *47*, 400; c) B. H. Moeckly, R. A. Buhrman, P. E. Sulewski, *Appl. Phys. Lett.* **1994**, *64*, 1427.
[17] R. F. Klie, J. P. Buban, M. Varela, A. Franceschetti, C. Jooss, Y. Zhu, N. D. Browning, S. T. Pantelides, S. J. Pennycook, *Nature* **2005**, *435*, 475.
[18] X. Zhang, H. Yu, G. He, W. Hu, J. Yuan, B. Zhu, K. Jin, *Phys. C* **2016**, *525–526*, 18.
[19] C. R. Rotundu, V. V. Struzhkin, M. S. Somayazulu, S. Sinogeikin, R. J. Hemley, R. L. Greene, *Phys. Rev. B* **2013**, *87*, 024506.
[20] P. Gao, Z. Kang, W. Fu, W. Wang, X. Bai, E. Wang, *J. Am. Chem. Soc.* **2010**, *132*, 4197.
[21] J. Brisbois, O.-A. Adami, J. I. Avila, M. Motta, W. A. Ortiz, N. D. Nguyen, P. Vanderbemden, B. Vanderheyden, R. B. G. Kramer, A. V. Silhanek, *Phys. Rev. B* **2016**, *93*, 054521.

Received: February 3, 2017
Revised: April 4, 2017
Published online:

